ELSEVIER

Physica A 228 (1996) 326–343

PHYSICA A

Spatio-temporal chaos and intermittency in a 1-dimensional energy-conserving coupled map lattice

C.I. Christov [1], G. Nicolis [2]

Center for Nonlinear Phenomena and Complex Systems, Université Libre de Bruxelles, Campus Plaine - CP 231, Boulevard du Triomphe, Bruxelles 1050, Belgium

Abstract

The Klein–Gordon equation with cubic nonlinearity (the ϕ^4 equation) is considered and an *energy-conserving* difference scheme is proposed for its solution. The scheme, extended to finite time increments and spacing, is then used to define a coupled map lattice for which an energy-like functional is conserved. The case of linear instability of the vacuum state is considered when this energy is not positive definite and found to lead, under certain additional conditions, to spatio-temporal chaos. The statistical properties of this type of solution such as probability densities and correlation functions are calculated. Strong intermittency, whereby the process wanders between two sub-manifolds, is found and studied in detail.

1. Introduction

Coupled maps are a useful model for understanding the onset of complex behaviour in spatially extended systems and for classifying the various types of regimes that may arise as the parameters measuring the strength of the coupling and the degree of nonlinearity are varied [1].

So far coupled map lattices have been studied predominantly in the context of dissipative dynamical systems, for which the evolution equations take the form

[1] On leave from National Institute of Meteorology and Hydrology, Bulgarian Academy of Sciences, Sofia, Bulgaria.

[2] To whom correspondence should be addressed.

SSDI 0378-4371(95)00429-7

$$x_{n+1}(r) = f(x_n(r)) + \frac{1}{d}\sum_{l\in A} D_l g(x_n(l)) , \tag{1.1}$$

where $r = \{r_j\}$ is the cell index in the lattice, l runs over the set of neighbors to which r is coupled including the cell itself, D_l being the corresponding coupling coefficient, and d is the coordination number. The coupling function g is model-dependent, whereas the function f accounts for the local dynamics in the absence of coupling. We shall refer to the type of coupling described by Eq. (1.1) as the "explicit" coupling.

Spatio-temporal complexity, particularly in the form of chaos, arises in energy conserving systems as well, where it is believed to play an important role in the foundations of statistical mechanics [2–4]. Ordinarily it is studied at the level of the evolution equations for the individual classical degrees of freedom (Hamilton's equations) or at the level of certain nonlinear partial differential equations (PDEs) possessing Hamiltonian structure and describing wave-like behaviour in continuous media. Our principal goal in the present paper is to develop a *discrete* coupled map lattice model for a spatially extended energy-conserving system and to analyze the behaviour of the solution generated for different ranges of parameter values.

Rather than proposing a heuristic model we begin with the space and time-discretized version of a nonlinear Hamiltonian PDE setting subsequently the time step and spacing (lattice parameter) equal to unity. The resulting equation differs substantially from (1.1), notably through the appearance of "implicit" coupling terms whereby certain coupling and locally nonlinear terms in the right-hand side are evaluated at time $n+1$ rather than n. The main advantage of this scheme is to secure conservation of energy at each stage of the process, although in the course of discretization the symplectic structure has been lost.

In Section 2 the nonlinear Klein–Gordon equation serving to generate the coupled map lattice is introduced and its main properties relevant to the present work are summarized.

In Section 3 an implicit difference approximation to the Klein–Gordon equation is proposed and shown to conserve the discrete version of the energy functional. Relations to soliton dynamics are also explored and the wave system obtained after soliton collisions is used as the initial condition for the subsequent Coupled Map Lattice (CML) calculations.

Section 4 presents the phenomenology of the regimes displayed by the CML model as revealed by numerical experiments, with special emphasis on spatio-temporal intermittency. The quantitative features of these regimes are further analyzed in Sections 5 and 6 where we discuss successively spatio-temporal correlations and probability density functions (p.d.f.).

The main conclusions are drawn in Section 7.

2. Nonlinear Klein–Gordon equation (ϕ^4 potential)

Consider the following generic equation arising in the study of nonlinear waves (see, e.g., [6,7]):

$$\frac{\partial^2 u}{\partial t^2} = \gamma^2 \frac{\partial^2 u}{\partial x^2} + \alpha_1 u + \alpha_3 u^3 \tag{2.1}$$

subject to the boundary conditions

$$u(-L_1, t) = u(L_2, t) = 0 . \tag{2.2}$$

The energy functional of (2.1) for the above boundary conditions reads

$$E \equiv \tfrac{1}{2} \int_{-L_1}^{L_2} \left[u_t^2 + u_x^2 - \alpha_1 u^2 - \alpha_3 \frac{u^4}{2} \right] \mathrm{d}x , \quad \text{with } \frac{dE}{dt} = 0 . \tag{2.3}$$

Notice that Eq. (2.1) is a general form of the so-called ϕ^4 potential equation since a term of quadratic nonlinearity can easily be removed through an appropriate change of the unknown function u. For different values of the parameters α_i, it describes different physical situations. In the sequel we will be interested in the case of an excitable system, for which α_1 and α_3 have opposite signs. Upon suitable scaling of the variables, Eq. (2.1) can then be recast in a form involving a single parameter,

$$\frac{\partial^2 u}{\partial t^2} = \frac{\partial^2 u}{\partial x^2} + \alpha(u - u^3) . \tag{2.4}$$

It is worth mentioning that if only the time or the spatial derivative is kept, Eq. (2.4) reduces to the non-forced Duffing oscillator. This dynamical system admits one trivial fixed point, $u = 0$, and two non-trivial ones, $u_\pm = \pm 1$. For $\alpha < 0$ the trivial fixed point is stable and one has a non-linearly excited system. When $\alpha > 0$, the trivial point loses its stability and the system is linearly excited, but the growth of the solution is saturated by the cubic nonlinear term. Because of its excitable nature the forced Duffing oscillator may exhibit chaotic behaviour. In the present context, the neighbor points in the spatially extended model serve in a sense as a forcing and some general features of the temporal evolution of the solution in a given spatial point like the onset of chaotic regime can be inferred from the experience one has from the forced Duffing oscillator. Note that Eq. (2.4) is believed *not* to be fully integrable [6].

In many instances, especially as far as the energy functional is concerned, the ϕ^4 equation is similar to another paradigm of nonlinear waves – the Boussinesq equations. It has been recently shown in [10] that the non-definiteness of the energy functional allows the amplitude of solution to grow up indefinitely in finite time (nonlinear blow-up). Numerically, the nonlinear blow-up can take place after an imperfect (inelastic) collision of two localized waves in the wake of which a residual signal is excited in the site of the bygone collision. If this signal happens to be of negative energy it is bound to grow and bring about the blow-up [11]. For the nonlinearly excited ϕ^4 equation we observe a slightly different route in the sense that after a collision of two localized waves the shape of solution quickly becomes chaotic prior to the blow-up. However, this chaotic stage is short-lived and no quantitative investigation of the statistical properties is possible. The solution resembles a breather with time-wise diverging spatially chaotic

amplitude. Because of this the nonlinearly excited case is of no interest for the present investigation.

The linearly excited case is quite an interesting one. It has no meaning in the framework of mechanical oscillators since it requires a spring that amplifies the motion in the direction of its compression (an "anti"-spring). However, it is possible to implement it in chains of electric circuits. It can also be derived as an amplitude equation for the buckling behaviour of thin elastic rods (t and x being the "slow" variables [12]) where the longitudinal compression of the rod plays the role of an "anti"-spring. One can expect nontrivial spatio-temporal dynamics from this system on the following grounds:

- The "vacuum state" $u = 0$ is linearly unstable, hence the system cannot reside near it.
- The nontrivial fixed points $u = \pm 1$ of the Duffing oscillator – to which our system reduces in the absence of coupling – are *not* solutions of the full coupled system, since a homogeneous state $u = \pm 1$ is precluded by the boundary conditions (2.2). On the other hand, in the excitable case, the boundary value problem for Duffing equation does not possess an unique solution (see [13] and references therein) and bifurcation may take place. Thus one is faced with a system with multiple stationary states.
- The system is excited in the initial moment of time by a finite amount of energy which remains constant during the evolution. At the same time, neighboring points will introduce perturbations to the motion of a given point. The slightest discrepancy between the input energy with the energy of an eventual regular steady spatial profile will make the latter impossible to be attained. The system is then expected to perform large excursions in its state space.
- As the cubic term is negative and energy finite such excursions will remain bounded. One may thus expect a wandering motion on a compact manifold which is precisely the type of complexity that one is confronted with in statistical mechanics.

3. Energy-conserving difference scheme and the associated Coupled Map Lattice (CML)

We now consider the discretized form (difference approximation) of our equation from which the implicitly coupled nonlinear map lattice will derive

$$\frac{u_i^{n+1} - 2u_i^n + u_i^{n-1}}{\tau^2} = \frac{1}{2}\left(\frac{u_{i+1}^{n+1} - 2u_i^{n+1} + u_{i-1}^{n+1}}{h^2} + \frac{u_{i+1}^{n-1} - 2u_i^{n-1} + u_{i-1}^{n-1}}{h^2}\right)$$
$$-\tfrac{1}{4}\alpha\left[(u_i^{n+1})^3 + (u_i^{n+1})^2 u_i^{n-1} + u_i^{n+1}(u_i^{n-1})^2 + (u_i^{n-1})^3\right]$$
$$+\tfrac{1}{2}\alpha\left(u_i^{n+1} + u_i^{n-1}\right). \tag{3.1}$$

The essential point here is the representation of the nonlinear term. Multiplied by $u^{n+1} - u^n$, it gives a term that brings about the conservation of energy (for general nonlinearity, see [15]). Adapting to this case the derivation from [14] it is straightforward to check that Eq. (3.1) conserves the *difference approximation for energy*,

$$E^{n+1/2} = \tfrac{1}{2}\sum_{i=2}^{N_p-1}\left(\frac{u_i^{n+1}-u_i^n}{\tau}\right)^2 - \alpha\left[(u_i^{n+1})^2+(u_i^n)^2\right] + \tfrac{1}{2}\alpha\left[(u_i^{n+1})^4+(u_i^n)^4\right]$$
$$+\frac{1}{2h}\sum_{i=1}^{N_p-1}\tfrac{1}{2}\left[\left(u_{i+1}^{n+1}-u_i^{n+1}\right)^2+\left(u_{i+1}^n-u_i^n\right)^2\right], \tag{3.2}$$

in the sense that $E^{n+1/2} = E^{n-1/2}$.

The dynamics defined by Eq. (3.1) involves three time steps which reflects the fact that it stems from a continuous-time dynamical system with Newton's law for the acceleration. The three-step structure of the map is instrumental for the behaviour discussed in what follows. Furthermore, the map is implicit and nonlinear, hence its numerical implementation requires linearization and iterations. The numerical procedure for achieving this is explained in detail in the appendix.

Some comments are in order here. First, despite the presence of nonlinear terms in u_i^{n+1} in the right-hand side of (3.1), the CML when implemented along the lines of the appendix actually generates a unique solution for any given initial condition. Second, the property of energy conservation of the discretized system is a strict one and its presence does not depend on the truncation error. The energy (3.2) is an approximation to the energy of the continuous system within the truncation error $O(\tau^2 + h^2)$, but its conservation when u_i^n satisfies Eq. (3.1) is secured independently of the values of the mesh parameters τ and h. This is a property of the *implicit scheme* and is to be contrasted with energy conserving schemes known from the literature where either the conservation holds for very small time steps (i.e., it is subject to the truncation error), or only for special relationship between the time increment τ and the spacing h. In this respect, in Ref. [8] the scheme of [9] was shown to possess a similar conservation property as ours only for $\tau = h/\sqrt{2}$. When this condition is not satisfied the energy functional contains terms of type $u^{n+1}u^n$ which do not bound the difference solution.

On the other hand, the presence of nonlinear terms on the new time stage $n+1$ does not allow us to check whether the phase space volume is preserved by the CML under consideration.

In principle, the above described conservative scheme can be started from an arbitrary initial condition and actually we have done numerous experiments with different initial conditions. In all of the cases reported here the CML "forgot" the initial condition and the time of the memory of the system did not depend on the specific shape of the initial condition. Localized conditions of type of "numerical δ-functions" were tested among the others but then the initial energy turned out not to be well controlled. We found it therefore useful to investigate the evolution of certain initial configurations in the form of localized waves whose energy can be evaluated analytically in the continuous case. In this respect it turns out that in both linearly and nonlinearly excitable cases, the nonlinear Klein–Gordon equation (2.1) admits a localized solution of *sech* type. In the moving frame $\xi = x - ct$ the solitary localized wave is given by

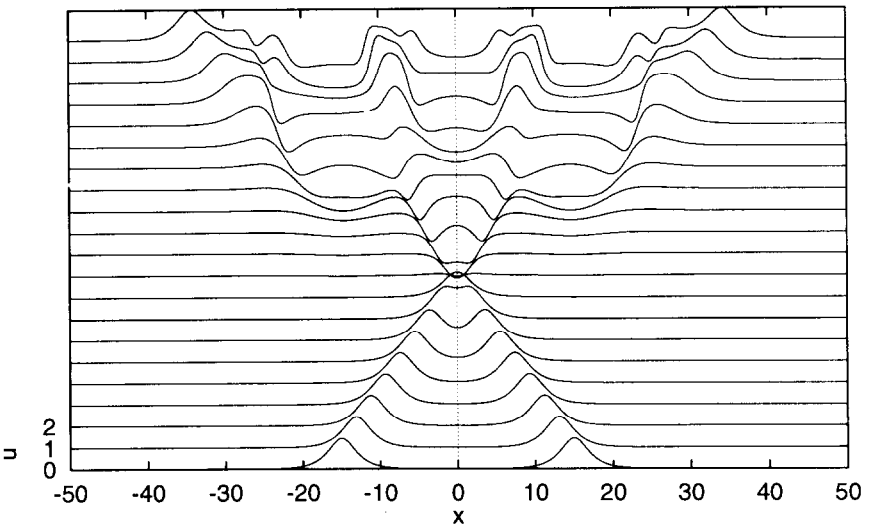

Fig. 1. The initial evolution of a system of two *sech*es for the linearly excited case. $c_l = -c_r = 1.9$, $\gamma = 1$, $\tau = 0.005$, $h = 0.05$, $N_p = 2001$ (time from 0 to 20 dimensionless units).

$$u = \frac{a}{\cosh b\xi}, \quad b = \sqrt{\frac{\alpha}{c^2 - \gamma^2}}, \quad a = \sqrt{2}. \tag{3.3}$$

To the best of our knowledge such localized solutions have not been the subject of thorough investigations. For $\alpha > 0$ the *sech*es are "supersonic" and for $\alpha < 0$ "subsonic". In the former case the vacuum state $u = 0$ is unstable and the *seches* can easily be destroyed by a small disturbance. In the latter their tails are linearly neutrally stable, but then the disturbances are amplified by the nonlinearity. After a collision, the deformation of the hump shape serves as finite-amplitude disturbance and eventually the nonlinear blow-up scenario develops. In this case the blow-up is connected with the improper sign of u^3 giving rise to the amplitude of u although the total energy is conserved.

Fig. 1 represents the head-on collision of two *sech*es obtained by numerical solution of the original PDE for $\tau = 0.005$ and $h = 0.05$ and $\alpha = 1$. The *sech*es could not survive and a complex wave pattern develops way before the humps reach the boundaries and recoil from them. After a number of reflections from the boundaries the solution eventually goes chaotic.

It is interesting to note that after collision, the humps change the signs of their amplitudes. In this respect they are very similar to the collision pattern of the kink solitons of Klein–Gordon and *sine*-Gordon equations. In fact, as seen on the figure, some kind of kinks of finite extent are being developed after the collision. They transform into another pattern of approximately kink shape, etc. Then the fore-runners reach the boundaries, recoil and the picture becomes even more complex until a fully developed spatial-temporal chaos takes place.

In what follows, the same *sech* shapes are used as initial conditions for the CML analysis. Naturally, they are no longer solutions of the discrete problem and for mesh

parameters of order of unity the mismatches can be very large. Nevertheless the estimate of the initial energy value of the system turns out to be quite good.

4. The CML: types of regime

In the sequel we shall focus entirely on the discrete map associated to the nonlinear Klein–Gordon equation, so we choose in Eq. (3.1) $\tau = 1$ and $h = 1$. Fixing the mesh parameters in this way makes the system depend solely on the parameter α. It is clear that if $\alpha \ll 1$ the influence of the boundaries will be much stronger, because of the increased relative importance of the spatial coupling. In fact, one can easily check that the discrete system for small α corresponds to a finite difference approximation of a continuous system with coefficients of order unity when the spacing h and time increment τ are proportional to $\alpha^{1/2}$.

One way to ensure balance between nonlinear term and spatial coupling is to take $\alpha \sim O(1)$. Unfortunately this increases the number of internal iterations (see the appendix) up to 40, because of the fast evolution of the solution: the function on a new time stage u^{n+1} differs point-wise significantly from u^n. An alternative way is to increase the number of lattice of points N_p. This increases the computational time, but because of the nonlinearity of the process the increase retains some dependence on the two parameters separately and does not depend solely on $\alpha^{-1/2}N_p$. We found the combination $\alpha = 0.08$, $N_p = 201$ to be optimal from the point of view of computational time and our longest time series have been collected for this set of parameters. We went as far as to 10^8 time steps.

First we need to check the spatial homogeneity of the process. We selected five different points of the lattice: the central point of number $N_c = (N_p - 1)/2$, two points situated at $N_c \pm N_c/4$ and two other points at $N_c \pm N_c/2$. We calculated probability distributions, covariances and correlations in these 5 points and compared them to each other. The differences between the quantities computed were less than 1% after the first 10^6 time steps. However, because of the strong intermittency (discussed below) the agreement does not improve significantly in the next couple of millions of time steps. In fact after 8×10^7 time steps the agreement was still only within 0.4%. Nevertheless, the process is sufficiently homogeneous to allow us to limit ourselves in the sequel to the computation of the various quantities of interest only for the central point (number N_c) of the chain.

The most conspicuous trait of the behaviour of the system under the above-defined conditions is that in the N_p-dimensional space the process wanders between two manifolds, each of which is close to one of the fixed points $u_\pm = \pm 1$ of the Duffing oscillator to which our system is reduced in the absence of spatial coupling. We use the notation $M^\pm$ for these two manifolds. The spatial average of the process (the spatial mean) can be used as an indicator for the solution being in the vicinity of the manifold M^+ or M^- depending on the sign of the mean value. Notice that, although $M^\pm$ do not cover the entire phase space, for practical purposes the system spends in the intermittent regime

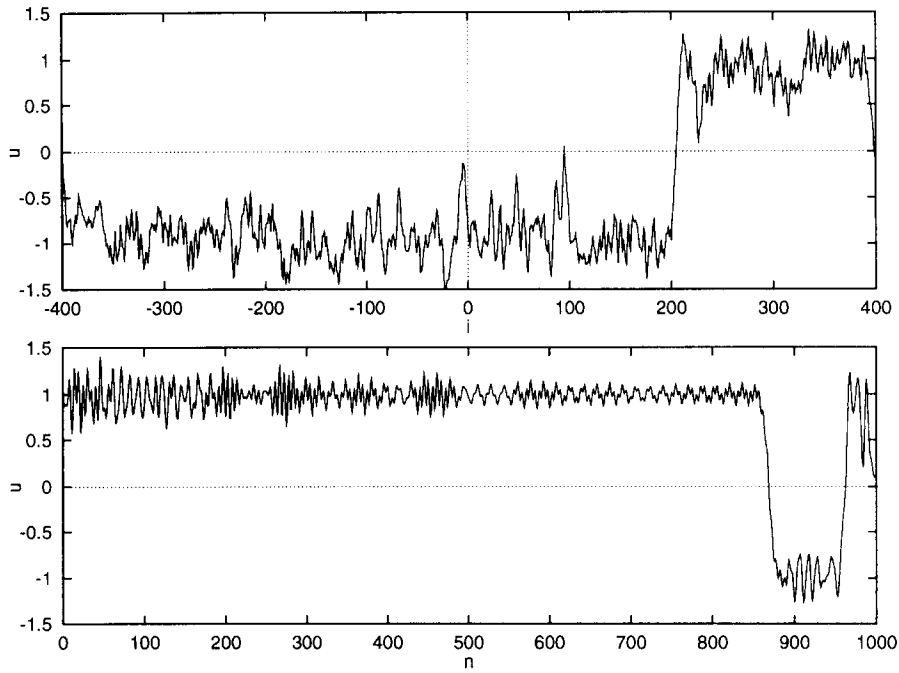

Fig. 2. The "sweep" throughout the space (up) and the "jump" in time (down) of the solution for $\alpha = 0.08$, $N_p = 801$, $E_0 = -1.907769682999$.

most of its time on either of these two manifolds.

The changes from one manifold to the other take place as very fast "sweeps" during which a jump starts from the one end of the chain and reaches the other in a relatively short time. Then the solution stays quite a long time in the vicinity of the manifold it has reached until another sweep takes place interchanging the state (manifold). We can refer to this process as *spatio-temporal intermittency*. Fig. 2 depicts the evolution of the variable after a certain transient time t_0 beyond which the switching process has started. The upper graph shows an instantaneous snapshot of the spatial profile when a "phase transition" from the manifold M^- to M^+ is protruding to the right. The lower graph depicts the time series for the central point which includes the time at which a transition took place. After the transition swept past it, the state of the central point changed from M^+ to M^-.

The transition process takes not more that 10^5 time steps, while the total length of the time series investigated was of order of 10^8. It can therefore be qualified as "fast". Note that in Fig. 2 we used a large number of spatial points $N_p = 801$ in order to make the transition slower for the sake of presentation. In fact, the sweeps are almost an order of magnitude faster for $N_p = 201$. The case presented in Fig. 2 is of relatively high initial energy $|E_0|$, the latter being conserved by the scheme up to the 13th digit. The separation of the time scale for the sweeps and the residence time near a manifold is even more pronounced for a lower absolute value of the energy of the system.

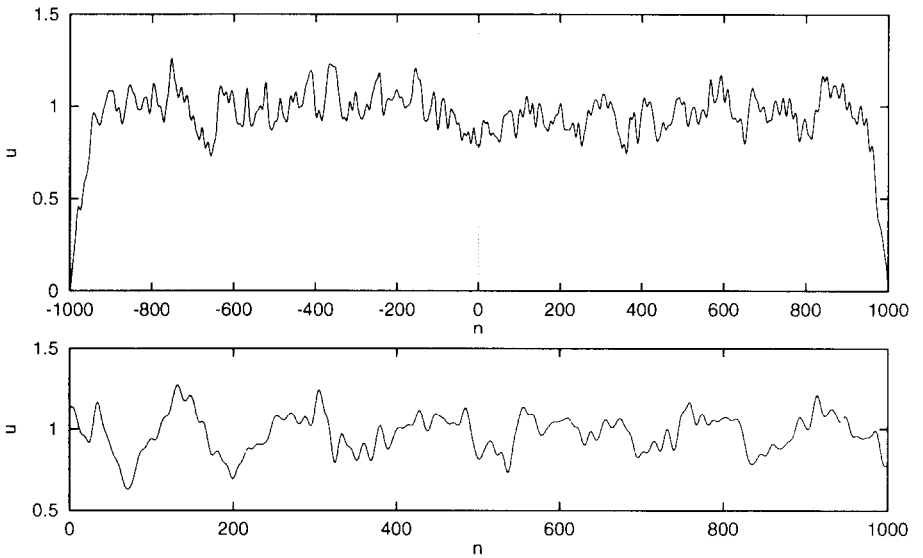

Fig. 3. The chaotic solution for $\alpha = 0.0008$, $N_p = 2001$, $E_0 = -0.04305981813542$ after 4.5×10^6 time steps. Spatial distribution (up); time series for the central point of lattice (down).

It is interesting to compare the instantaneous spatial and temporal profiles for different α. In Fig. 3 the profiles for $\alpha = 0.0008, N_p = 2001$ are presented. As could have been expected, the solution for small α resembles more the difference solution to the original continuous problem in the sense that though strictly speaking the shape of function u is non-differentiable it is considerably smoother than in the case $\alpha = 0.08$. Another difference between the cases of Figs. 2 and 3 is that in the latter the absolute value of energy of the system is much lower than in the former and the amplitude of the excursion of the process around one of the manifolds is therefore of significantly lesser amplitude. As a result the process stays only near one of the manifolds (M^+ as it turns out for the result presented in the figure – for 5×10^6 time steps) and does not have enough energy to start a phase transition toward the other manifold. Thus the intermittency property is lost for $|E_0| \ll 1$.

The wide separation between the residence time of each of the states and the transition between states in the intermittent regime suggests to introduce a new, coarse-grained variable $I(n)$ playing the role of a *characteristic function* for locating the system on one of the manifolds M^+ or M^-. Specifically, we define

$$I(n) = \begin{cases} 1 \text{ if } \langle u \rangle > 0, \\ -1 \text{ if } \langle u \rangle < 0, \end{cases} \qquad \langle u \rangle = \sum_{i=2}^{N_p - 1} u_i^n . \tag{4.1}$$

In Fig. 4 the evolution of the characteristic function with time is shown. The pattern resembles a fractal, because the jump times of the process are of such different magnitudes that after a zoom the picture is quite similar. As the system gets smaller (strong influence of boundaries) while keeping the energy the same per lattice point,

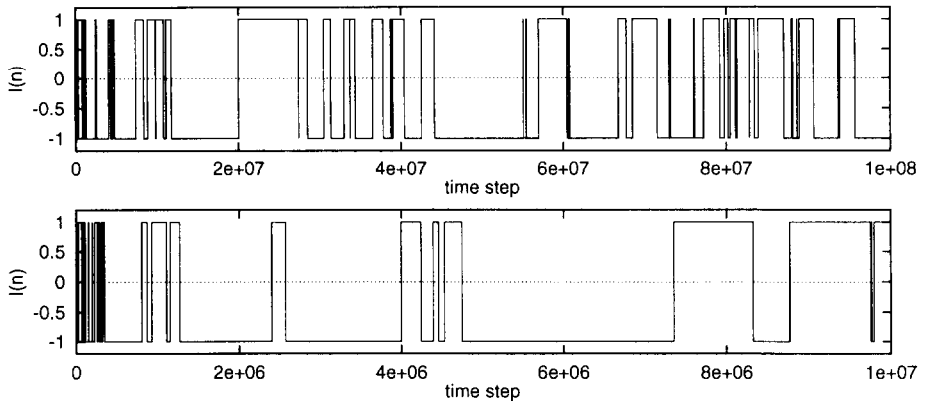

Fig. 4. The intermittency of the coarse-grained parameter for $\alpha = 0.08$, $N_p = 201$ after 10^8 iterations (up) and a zoom (down).

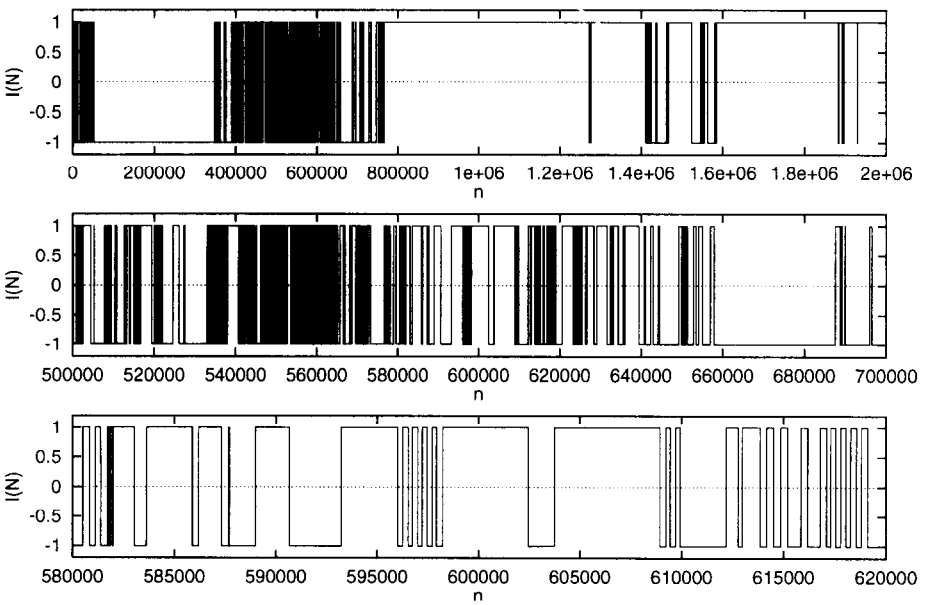

Fig. 5. Intermittency plot (up) with two zooms for $\alpha = 0.0008$, $N_p = 201$ after 2×10^6 time steps.

intermittency subsists, but in a qualitatively different form. Now the average times for transitions from one state to another are much shorter, as can be seen in Fig. 5.

5. Correlation functions

In order to characterize the complexity of the behaviour summarized above we compute, in this section, a number of statistical indicators easily accessible from the multidi-

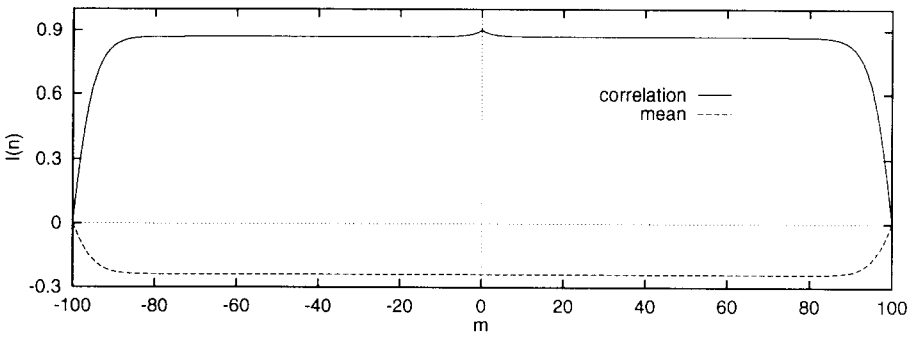

a) spatial correlation after 10^8 time steps;

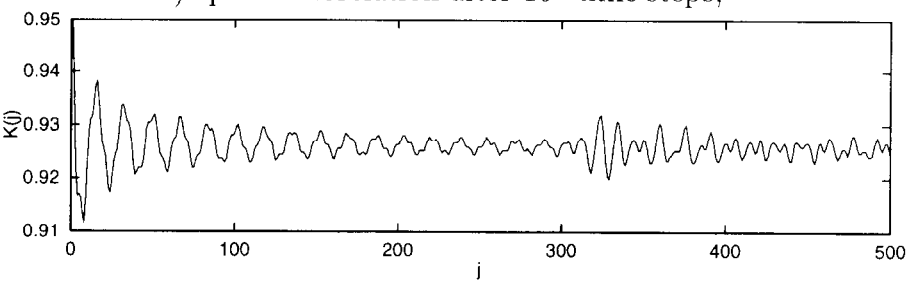

b) time correlation after $2.7 \cdot 10^7$ time steps;

Fig. 6. Averaged characteristics of the solution for $\alpha = 0.08$, $N_p = 201$.

mensional time series data. We discuss the behaviour of the time averages, the two-point spatial or temporal moments and the associated correlation functions.

For the N_p-dimensional vector process we define these quantities as

$$A(m) = \frac{1}{N_t} \sum_{n=1}^{N_t} u^n_{N_c+m} \quad \text{(time average)}, \tag{5.1}$$

$$M(m) = \frac{1}{N_t} \sum_{n=1}^{N_t} u^n_{N_c} u^n_{N_c+m} \quad \text{(two-point spatial covariance)}, \tag{5.2}$$

$$K(m) = M(m) - A(0)A(m) \quad \text{(two-point spatial correlation)}, \tag{5.3}$$

$$M(j) = \frac{1}{N_t} \sum_{n=1}^{N_t} u^n_{N_c} u^{n+j}_{N_c} \quad \text{(two-time covariance)}, \tag{5.4}$$

$$K(j) = M(j) - A^2(0) \quad \text{(two-time correlation)}, \tag{5.5}$$

where N_t is the number of time steps which plays the role of the number of realizations in an ensemble.

The mean and spatial autocorrelation functions are shown in Fig. 6a.

We see that the process "forgets" the boundary conditions beyond a number of 25 points near each boundary. Our experience with some other sets of parameters shows

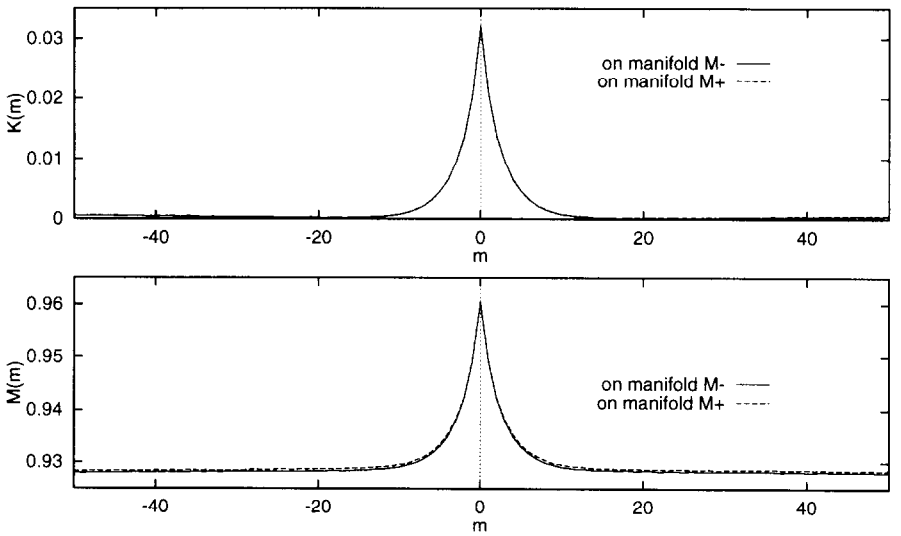

Fig. 7. Comparing the averaged characteristics as calculated on the two different manifolds for $\alpha = 0.08$, $N_p = 201$, $E_0 = 0.4553256662888$: correlation function (up); covariance (down).

that a safe estimate for the number of points needed at each boundary as a buffer is $100\alpha^{-1/2}$. In this respect it is worth noting that whereas fixed boundary conditions allow one to reach this type of insight, the use of the somewhat more familiar (in this context) periodic boundary conditions would have introduced artificial long range correlations which would subsequently need to be removed.

Due to the intermittency the spatial correlation function $K(m)$ does not decay at large distances. This behaviour is also shared by the temporal correlation function $K(j)$, see Fig. 6b. Notice that the two-point spatial correlation is a monotonous function (in each half of the interval) while the two-time correlation is oscillating, hinting at the presence in the process of a part that is periodic in time modulating the chaotic profile.

It is instructive to calculate the two-point quantities on the different manifolds simply by taking the time averages when the coarse-grained variable $I(n)$ is positive or negative, respectively. Fig. 7 shows the comparison between spatial correlation and covariance functions as calculated on the two different manifolds M^- and M^+. They are in very good agreement with each other which confirms that the scheme respects the symmetry of the original equation (changing u to $-u$ does not change the results). The correlations tend now fairly well to zero for large separation of the arguments. The small residual value is presumably due to to the roughness of the criterion of selection of the variable $I(n)$.

For very small $\alpha = 0.0008$ and small energy $|E_0|$, the spatial mean and autocorrelation function for the manifold M^+ are shown in Fig. 8. Now the number of points needed by the process in order to "forget" the boundaries and to regain the spatial homogeneity is of order of 250 at each boundary which confirms the $\alpha^{-1/2}$ scaling for the number of points required for homogeneity.

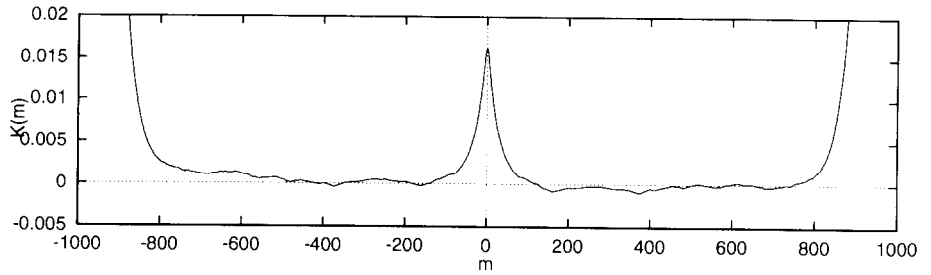

Fig. 8. Spatial correlation and mean of the solution for $\alpha = 0.0008$, $N_p = 2001$ after 4.5×10^6 time steps spent by the process in the vicinity of M^+.

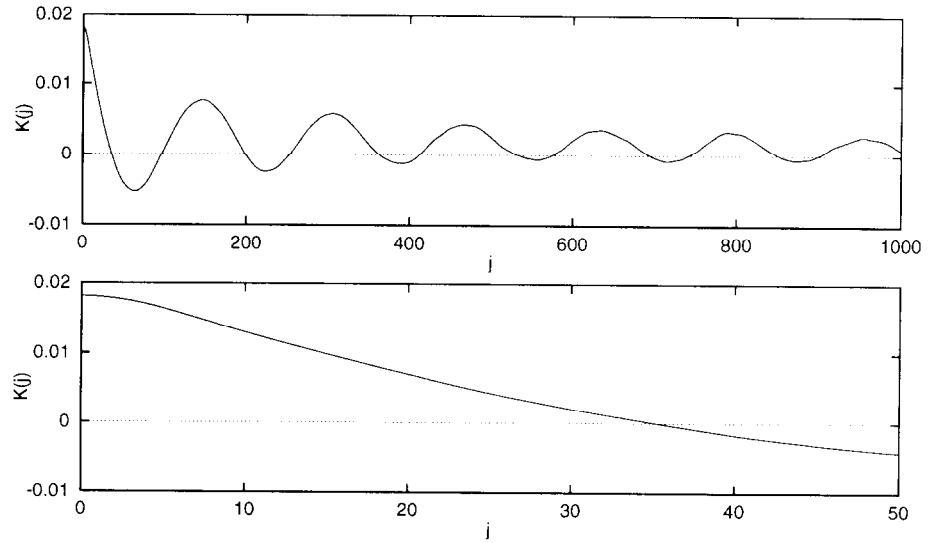

Fig. 9. Time correlation of the solution for $\alpha = 0.0008$, $N_p = 2001$ on M^+ after 4.5×10^6 time steps spent by the process in the vicinity of M^+ (up) and a zoom near the origin (down).

The temporal correlation shown in Fig. 9 is considerably smoother than in the previous case. This could be expected since in a conservative, continuous time-reversible dynamics time autocorrelation functions are differentiable at the origin. It is interesting to mention that the magnitude of the correlation maximum differs about 30% from the previous case. This is directly connected to the lower energy level.

Finally, we present the correlation functions for the case of very strong influence of the boundaries $\alpha = 0.0008$ but for a large enough absolute value of the energy to allow for intermittency. According to the estimate from the previous examples one can expect that for $N_p = 201$ the boundary regions may overlap. Fig. 10 represents the correlation function for M^- (the result for M^+ being the same up to a change of sign for the mean profile). One sees that spatial homogeneity is no longer observed in the interval, i.e. the influence of the boundaries is very strong. Still, the process remains chaotic. Even the strong influence of the boundary is not sufficient to stabilize the system into a spatially regular pattern. Note that in this case the coarse-grained variable (4.1) is no longer a

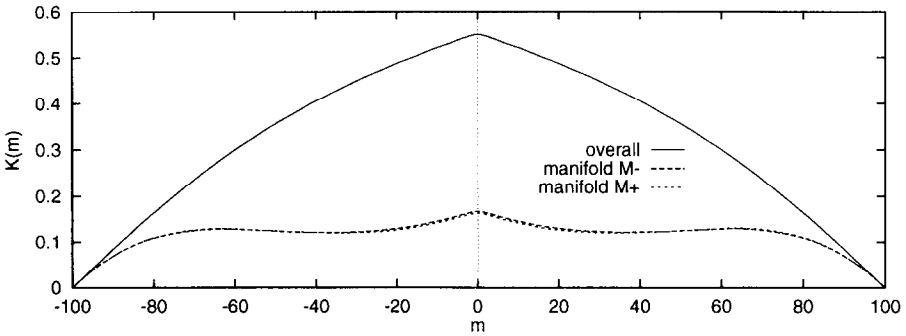

Fig. 10. Spatial correlation for $\alpha = 0.0008$, $N_p = 201$ after 2×10^6 time steps.

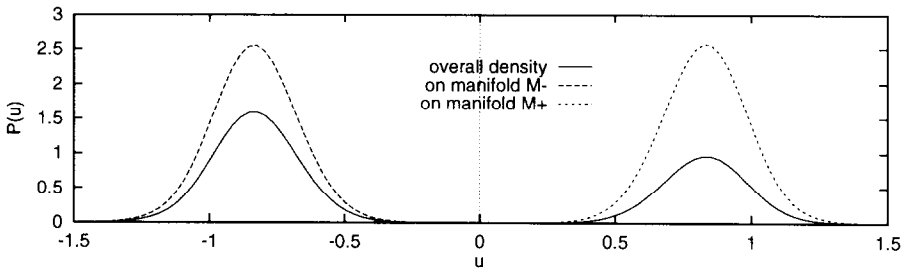

Fig. 11. Probability density for $\alpha = 0.08$, $N_p = 201$, $E_0 = 0.4553256662888$ after 8×10^7 time steps.

good criterion for phase transition since now it is much more often close to zero and the residence time is not so sharply defined.

6. Probability densities

We begin with the case $\alpha = 0.08$. Fig. 11 depicts the probability density in the central point of the lattice (continuous line). The most conspicuous feature of this probability density is its bimodality.

The dashed lines shown in Fig. 11 are the probabilities for the two different manifolds accumulated separately. As it could have been expected each of them is unimodal with maximum in the vicinity of the points $u = +1$ or $u = -1$, respectively. It is interesting to mention that even after 8×10^7 time steps the process does not settle to symmetric distribution. For this period of time the system stayed roughly about 65% of the time near M^- and only 35% – near M^+. Notice that the probability distributions decay fairly sharply as functions of u.

The probability distribution for the case shown in Fig. 3 is given in Fig. 12 and is seen to be unimodal around the point $u = 1$, reflecting the loss of intermittency as pointed out already in Section 4. It is also steeper and with shorter span since the lower energy entails a more limited wandering of the process in state space.

The case of strong influence of the boundary is presented in Fig. 13a. In the light

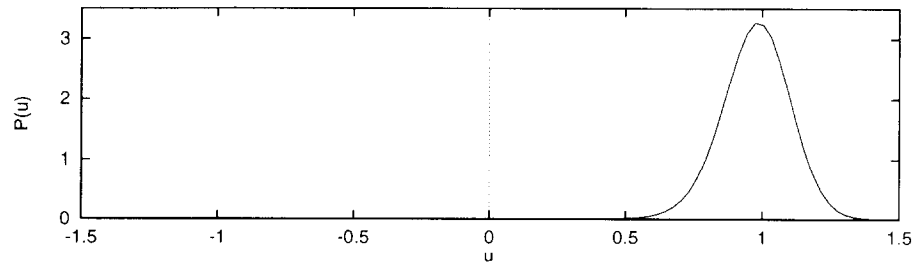

Fig. 12. Probability density for $\alpha = 0.0008$, $N_p = 2001$, $E_0 = -0.04305981813542$ after 4.5×10^6 time steps.

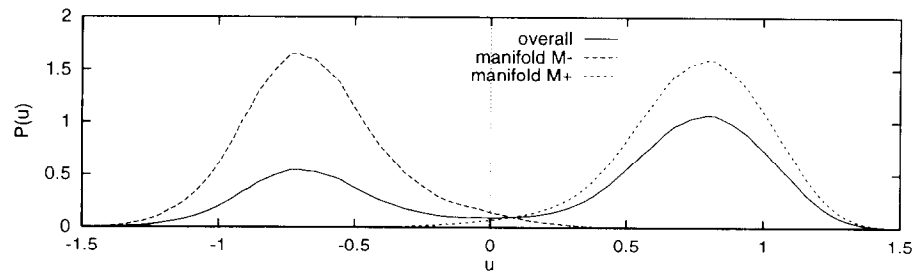

a) $E_0 = -0.03098040741488$

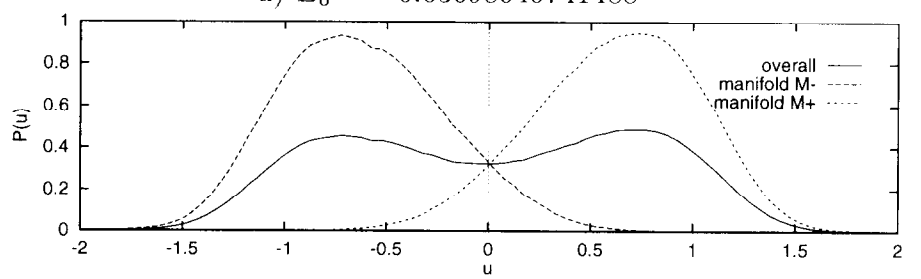

b) $E_0 = -0.2652409827415$

Fig. 13. Probability density in the central point of map for $\alpha = 0.0008$, $N_p = 201$, after 2×10^6 time steps.

of what has been said in the previous section about the influence of the boundaries one can expect different behaviour of the system if one takes a smaller number of lattice points, because of the overlapping of the two "boundary regions". One could have even expected that the p.d.f. of the process may have been significantly deformed and bimodality would be lost. Fig. 13a shows the result for the probability distribution in the central point. Although significantly deformed the p.d.f. is still bimodal, at least for the energy level considered.

For higher energy levels the deformation of the p.d.f. becomes more pronounced and approaches a unimodal form (Fig. 13b). Increasing the energy further ($|E_0| > 0.5$) yields for this set of parameters a spatially chaotic profile that is virtually periodic in time. The p.d.f. becomes then fully unimodal.

The behaviour summarized above suggests that for the square of the function u one

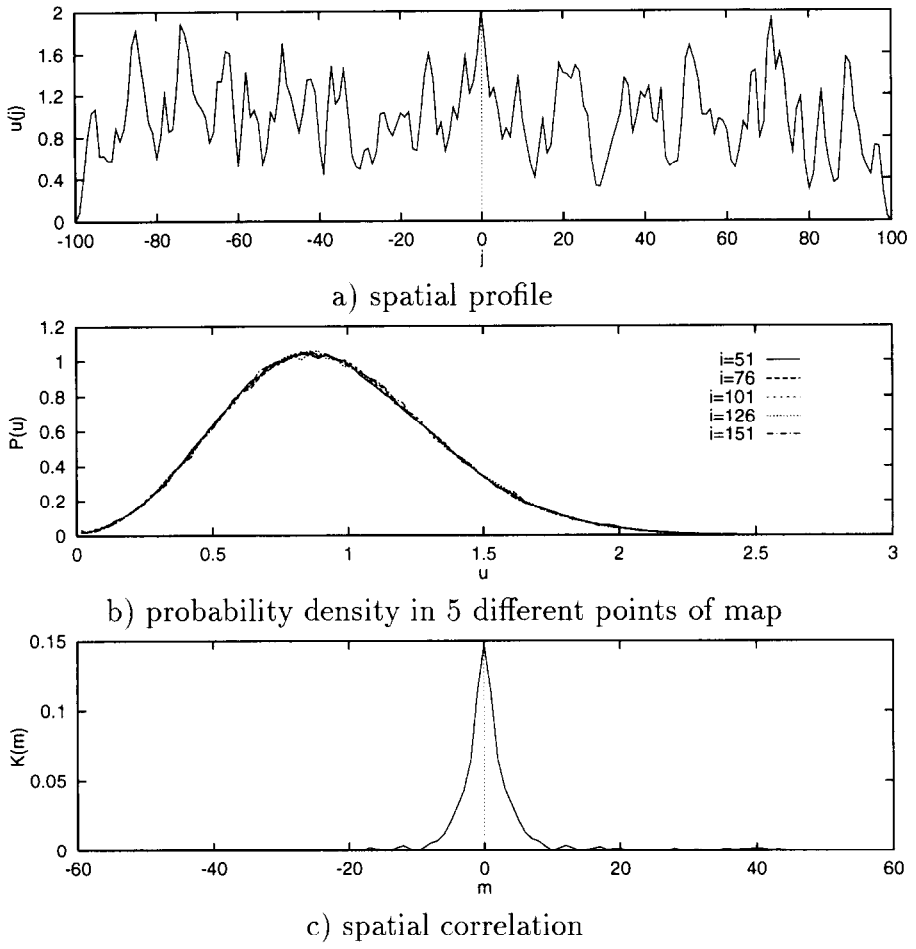

Fig. 14. Results in terms of u^2 for $\alpha = 0.08$, $N_p = 201$.

may have a unimodal distribution. A typical spatial profile of u^2 is shown in Fig. 14a. Fig. 14b shows that the corresponding probability distribution is indeed unimodal. It is interesting to mention here that the probability that u^2 stays near zero is not negligibly small. This is due to the fact that for small u values taking the square yields even smaller values for u^2, thus increasing the number of cases where u^2 is a small quantity. Finally, the correlation function for u^2 decays to zero as seen in in Fig. 14c.

7. Conclusions

In this paper, starting from the nonlinear Klein–Gordon equation with cubic nonlinearity we generated a fully energy-conserving coupled map lattice (CML). This space- and time-discrete dynamical system turned out to give rise to a very rich behaviour,

particularly in the form of spatio-temporal chaos. Depending on the system size, the value of the initial energy and the sole governing intrinsic parameter α, the type of chaos observed could vary from smooth, small amplitude aperiodic spatio-temporal oscillations to sharp large-amplitude ones whereby the system switches intermittently between two sub-manifolds of its state space. The analysis of space- and time- correlation functions and of probability densities provided useful insights on the complexity of these dynamical behaviors. In particular, it turned out that intermittency is manifested through a bimodality of the probability distribution and long tails in the spatial and temporal correlation functions.

The CML developed in this work is a flexible model allowing one to identify, at reasonable computational cost, a variety of phenomena that would be less accessible in traditional space- or time-continuous Hamiltonian systems. Of special interest from the point of view of statistical mechanics is the regime of strong intermittency. The system appears as metrically intransitive for a substantial period of time, yet for very long times transitivity and ergodicity are established, albeit with weak mixing properties as witnessed by the lack of decay of the correlation functions. As the parameters are varied bimodality generally disappears and mixing is fully secured. These points will be taken up and developed further in a forthcoming communication devoted to the mechanical analog of the model analyzed in the present paper.

Acknowledgements

This work is supported in part by the European Commission under the Human Capital and Mobility Program – Grant ERBCHBICT940982 and contract ERBCHRXCT930107 – and by the Belgian Federal Services of Scientific, Technical and Cultural Affairs under the Pôles d'Attraction Interuniversitaires Program.

The authors wish to thank an anonymous referee for helpful remarks.

Appendix A. Internal iterations

The difference scheme/coupled map introduced in Section 3 is nonlinear and can only be implemented by means of iterations. We use for this purpose the following linearized scheme:

$$\frac{u_i^{n+1,k}-2u_i^n+u_i^{n-1}}{\tau^2}=\frac{1}{2}\left(\frac{u_{i+1}^{n+1,k}-2u_i^{n+1}+u_{i-1}^{n+1}}{h^2}+\frac{u_{i+1}^{n-1}-2u_i^{n-1}+u_{i-1}^{n-1}}{h^2}\right)$$
$$-\frac{1}{4}\alpha\left\{\left[(u_i^{n+1,k-1})^2+u_i^{n+1,k-1}u_i^{n-1}+(u_i^{n-1})^2\right]u_i^{n+1,k}+(u_i^{n-1})^3\right\}$$
$$+\frac{1}{2}\alpha\left(u_i^{n+1,k}+u_i^{n-1}\right), \qquad \text{(A.1)}$$

which requires inversion of a three-diagonal system. To this end we employ a specialized solver developed by one of the present authors [16].

The inner iterations start from the functions obtained at the previous time stage $u_i^{n+1,0} = u_i^n$, and are terminated at a certain $k = K$ when

$$\max |u_i^{n+1,K} - u_i^{n,K-1}| \leq 10^{-13} \max |u_i^{n+1,K}| .$$

The value 10^{-13} is selected to be large enough in comparison with the round-off error 10^{-14}. In general, the number of iterations K depends on the size of time increment or for $\tau = h = 1$ on parameter α. After the inner iterations converge one obtains, in fact, the solution for the new time stage $n + 1$ of the nonlinear conservative difference scheme, namely $u_i^{n+1} \stackrel{\text{def}}{=} u_i^{n+1,K}$.

References

[1] K. Kaneko, Physica D 34 (1989) 1.
[2] I. Prigogine, From Being to Becoming (Freeman, San Francisco, 1980); A. Lichtenberg and M. Liberman, Regular and Stochastic Motion (Springer, Berlin, 1983).
[3] L. Bunimovich and Ya. Sinai, Comm. Math. Phys. 78 (1980) 247.
[4] L. Bunimovich and Ya. Sinai, Comm. Math. Phys. 78 (1980) 479.
[5] A.R. Bishop, J.A. Krumhansl and S.E. Trullinger, Solitons in condensed matter: a Paradigm, Physica D 1 (1980) 1.
[6] F. Calogero and A. Degasperis, Spectral Transform and Solitons: Tools to Solve and Investigate Nonlinear Evolution Equations, Vol. 1 (North Holland, Amsterdam, 1982).
[7] A.C. Scott, F.Y.F. Chu and D.W. McLaughlin, Proc. IEEE 61 (1973) 1443.
[8] R. Glassey and J. Shaeffer, Math. Comput. 56 (1991) 87.
[9] W. Strauss and L. Vasquez, J. Comp. Phys. 28 (1978) 271.
[10] S.K. Turitzyn, Phys. Rev. E 47 (1993) R13.
[11] C.I. Christov and M.G. Velarde, Int. J. Bifurcation Chaos 4 (1994) 1095.
[12] C.G. Lange and A.C. Newell, SIAM J. Appl. Math. 21 (1971) 605.
[13] M. Feibig-Wittmaack, J. Appl. Math. Phys. (ZAMP) 42 (1991) 445.
[14] C.I. Christov, in: Fluid Physics, M.G. Velarde and C.I. Christov, eds. (World Scientific, Singapore, 1995) p. 403.
[15] C.I. Christov, in: Proc. ICFD V, Oxford 1995, W.K. Morton and M.J. Baines, eds. (Oxford University Press, Oxford, 1995).
[16] C.I. Christov, Gaussian elimination with pivoting for multidiagonal systems, Report 4, University of Reading (1994).